High throughput exploration of $Zr_xSi_{1-x}O_2$ dielectrics by evolutionary first-principles approaches

Jin Zhang [a,b], Qingfeng Zeng [a,*], Artem R. Oganov [a,b,c], Dong Dong [a], Yunfang Liu [a]

[a] *Science and Technology on Thermostructural Composite Materials Laboratory, and International Center for Materials Discovery, School of Materials Science and Engineering, Northwestern Polytechnical University, Xi'an, Shaanxi 710072, People's Republic of China*
[b] *Department of Geosciences, Center for Materials by Design, and Institute for Advanced Computational Science, State University of New York, Stony Brook, NY 11794-2100, USA*
[c] *Moscow Institute of Physics and Technology, Dolgoprudny, Moscow Region 141700, Russia*

A B S T R A C T

The high throughput approaches aim to discover, screen and optimize materials in a cost-effective way and to shorten their time-to-market. However, computational approaches typically involve a combinatorial explosion problem, to deal with which, we adopted hybrid evolutionary algorithms together with first-principle calculations to explore possible stable and metastable crystal structures of ZrO_2–SiO_2 dielectrics. The calculation reproduced two already known structures ($I4_1/amd$-$ZrSiO_4$ and $I4_1/a$-$ZrSiO_4$) and predicted two new thermodynamically metastable structures Zr_3SiO_8 ($P\bar{4}3m$) and $ZrSi_2O_6$ ($P\bar{3}1m$). At ambient pressure, the only thermodynamically stable zirconium silicate is $I4_1/amd$-$ZrSiO_4$ (zircon). Dynamical stability of the new phases has been verified by phonon calculations, and their static dielectric constants are higher than that of the known phases of $ZrSiO_4$. Band structure, density of state, electron localization function and Bader charges are presented and discussed. The new metastable structures are insulators with the DFT band gaps of 3.65 and 3.52 eV, respectively. Calculations show that $P\bar{4}3m$-Zr_3SiO_8 has high dielectric constant ($\sim$20.7), high refractive index ($\sim$2.4) and strong dispersion of light. Global optimization of the dielectric fitness (electric energy density) shows that among crystalline phases of ZrO_2–SiO_2, maximum occurs for $I4_1/a$-$ZrSiO_4$.

© 2014 Elsevier B.V. All rights reserved.

1. Introduction

To speed up the process of materials discovery, the high throughput concept has been introduced into the recent Materials Genome Initiative project [1–3]. Besides high throughput (combinational) experiments, computational approaches could further accelerate the discovery, screening and optimization process for complex materials systems. Finding the global optimum of both the energy and any other physical property is essentially a combinatorial problem. However, very large numbers of atomic combinations result in a very complex structure–property hypersurface, in which it could be very difficult to locate the global and relevant local minima. Here we apply state-of-the-art computational methodologies to optimize, through structural or chemical modification, the properties of zircon ($ZrSiO_4$), a well-known material possesses many useful chemical and physical properties that enable it to play a significant role as a versatile functional material in

both the metallurgical industry and the electronic industry. $ZrSiO_4$ has exceptional low oxygen permeation rate, low thermal conductivity, and low coefficient of thermal expansion in the temperature range from room temperature to 1500 °C as well as good thermal shock resistance, which makes it an important candidate for high-temperature structural materials and anti-oxidation protective coatings [4–6]. High refractive index (1.93–2.01) and strong dispersion make $ZrSiO_4$ a preferred opacifier in the ceramic glaze industry [7]. In the electronics industry, it excites an increasing interest in the search for high-κ dielectrics (i.e. materials with high dielectric constant) for the sake of avoiding direct tunneling current induced by the continuous minimization of complementary metal-oxide semiconductor (CMOS) devices [8]. Like our previously investigated HfO_2–SiO_2 system [9], the ZrO_2–SiO_2 system is promising for use as a gate dielectric material in the microelectronic industry because of its relatively higher dielectric permittivities (7.9–13) compared to α-quartz (3.9), wide band gap, large band offsets and excellent interfacial stability with Si [10].

The electronic properties of zircon are well known: its static dielectric constant is around 12.7 [11], and its bandgap is about 6.5 eV [12]. Although other zirconium silicates are also known, so
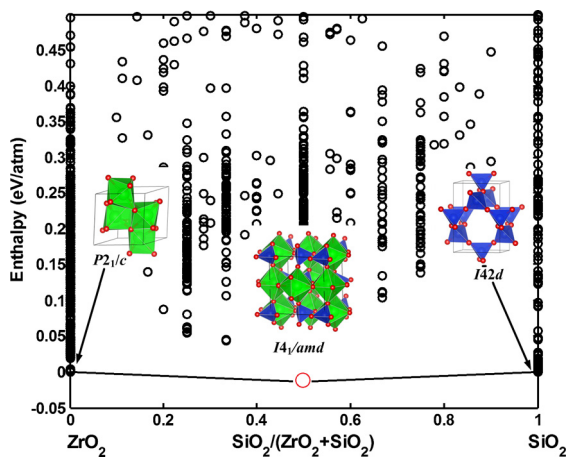
Fig. 1. Thermodynamics of ZrO$_2$–SiO$_2$ compounds found by USPEX.

far most experimental and theoretical studies have focussed on the thermodynamically stable one, zircon (space group $I4_1/amd$) and the amorphous structures, but much less attention has been paid to other possible crystal structures of ZrO$_2$–SiO$_2$ compounds and their corresponding electronic and dielectric properties.

2. Computational methodology

To find optimal compositions and the corresponding crystal structures, we performed variable-composition search of the ZrO$_2$–SiO$_2$ system using the USPEX code [13–16], in conjunction with first principles structural relaxations using density functional theory (DFT) within the Perdew–Burke–Ernzerhof (PBE) generalized gradient approximation (GGA) [17], as implemented in the VASP package [18]. We employed projector augmented wave (PAW) [19] potentials with four valence electrons for Zr ($4d^25s^15p^1$), four for Si ($3s^23p^2$), and six for O ($2s^22p^4$). The wave functions are expanded in a plane-wave basis set with a kinetic energy cutoff of 600 eV and Monkhorst–Pack meshes [20] for Brillouin zone sampling with reciprocal space resolution of $2\pi \times 0.06$ Å^{-1}.

We used the VASP package to carefully reoptimize the obtained structures before calculating the band structure, electronic density of state (DOS), static dielectric constant and optical properties of Zr$_3$SiO$_8$ and ZrSi$_2$O$_6$. For these relaxations, we also used the plane-wave cutoff of 600 eV. A $9 \times 9 \times 9$ k-point grid was used to relax the structures and a $19 \times 19 \times 19$ k-point grid was employed to calculate the DOS. Phonopy package [21] was used to calculate the phonon dispersion curves using $2 \times 2 \times 2$ supercells. Bader analysis was performed using the code [22,23].

3. Results and discussions

3.1. Crystal structure prediction and structural properties

The variable-composition evolutionary algorithm [13,14], which has been applied in a number of studies [24–26], can efficiently predict stable and metastable compounds (and their structures) in multicomponent systems. In our variable-composition searches, all possible ZrO$_2$–SiO$_2$ compounds (with up to 30 atoms in the unit cell) were allowed, and calculations were set to run up to 40 generations; 80 structures were randomly produced as the initial generation and all subsequent generations contained 40 structures. 40% of the new structures were produced by a heredity operator, 20% by softmutation, 20% by random generation, and 20% by transmutation. The thermodynamic stability of the structures was analyzed using the convex hull construction (Fig. 1) that was

also used to define "fitness" for each structure in the evolutionary search.

Our crystal structure prediction gave four distinct stable or metastable crystal structures of zirconium silicates among a number of crystalline forms of ZrO$_2$–SiO$_2$ at ambient pressure and zero Kelvin: ZrSiO$_4$ ($I4_1/amd$), ZrSiO$_4$ ($I4_1/a$), Zr$_3$SiO$_8$ ($P\bar{4}3m$) and ZrSi$_2$O$_6$ ($P\bar{3}1m$). Among these four structures, $P\bar{4}3m$-Zr$_3$SiO$_8$ [Fig. 2(a)] and $P\bar{3}1m$-ZrSi$_2$O$_6$ [Fig. 2(b)] that have not been previously reported. The enthalpies of formation of the all the structures discovered by USPEX are shown in Fig. 1. Our calculations confirm that zircon is the only thermodynamically stable zirconium silicate, while the other three phases ($I4_1/a$-ZrSiO$_4$, $P\bar{4}3m$-Zr$_3$SiO$_8$, $P\bar{3}1m$-ZrSi$_2$O$_6$) are metastable. For ZrO$_2$, the $P2_1/c$-ZrO$_2$ phase (baddeleyite) is found to be the most thermodynamically stable phase at normal conditions in the framework of DFT–GGA, which agrees with experiments [27]. $I\bar{4}2d$-SiO$_2$ (a beta-cristobalite phase) has the lowest energy in the framework of DFT–GGA, which conflicts with the fact that α-quartz ($P3_121$) is the stable form at normal conditions. This error of DFT–GGA for SiO$_2$ has been reported before [28], and has roots in the tendency of the GGA to overestimate stability of lower-density structures. The computed energy difference between $I\bar{4}2d$-SiO$_2$ and $P3_121\alpha$-quartz is, however, very small – 0.01 eV/atom. In addition to the search for stable phases, we have also performed variable-composition searches targeting the maximum value of the electric energy density (see below).

Structural parameters and energetics of $I4_1/amd$-ZrSiO$_4$, $I4_1/a$-ZrSiO$_4$, $P\bar{4}3m$-Zr$_3$SiO$_8$ and $P\bar{3}1m$-ZrSi$_2$O$_6$ are presented in Table 1. Phonon calculations show the absence of imaginary phonon frequencies [Fig. 2(c) and (d)], which verifies the dynamical stability of these phases.

3.2. Electronic structure

Both Zr$_3$SiO$_8$ ($P\bar{4}3m$) and ZrSi$_2$O$_6$ ($P\bar{3}1m$) have pronounced band gaps (DFT gaps are close to 4.0 eV, Fig. 3). The highest occupied bands of Zr$_3$SiO$_8$, as shown in Fig. 3(a), have high occupancy of both Zr-d and O-p orbitals, which implies a strong hybridization of Zr-d and O-p valence states. The highest occupied states in ZrSi$_2$O$_6$ [Fig. 3(b)] are derived predominantly from O-p orbitals.

Electron localization function (ELF) is useful in revealing information about the bonding features and valence electron configuration of atoms in a compound [29]. ELF plots [Fig. 3(c) and (d)] show that valence electrons localize on O atoms. To obtain further insight, we analyzed total electron density using the Atoms in Molecules (AIM) theory developed by Bader [22,23]. For Zr$_3$SiO$_8$, Zr atoms have a charge +2.33, i.e. contribute 2.33 electrons/atom, Si atoms contribute 3.15 electrons/atom while O1 atoms get 1.42 electrons/atom and O2 get 1.11 electrons/atom. Thus, a substantial degree of ionicity exists in Zr$_3$SiO$_8$. Fig. 3(d) shows that valence electrons in ZrSi$_2$O$_6$ are mainly concentrated around O atoms. Bader charge analysis of ZrSi$_2$O$_6$ indicates that Zr atoms contribute 2.42 electrons/atom, Si atoms contribute 3.19 electrons/atom while O atoms get 1.46 electrons/atom, which again shows a significant degree of ionicity of bonding.

3.3. Dielectric and optical properties

To explore the high-κ materials with high electric energy storage capacity, we also performed variable-composition USPEX searches but with a fitness function related to the electric energy density [9]. It is expressed by Eq. (1), where E_{BI} is the intrinsic breakdown field, E_g is the bandgap, κ is the average static dielectric constant and $E_{gc} = 4$ eV, which refers to the critical bandgap value separating materials into semiconductors (below E_{gc}) and insulators (above E_{gc}). For the semiconductors, $\alpha = 3$, while for the insulators, $\alpha = 1$.
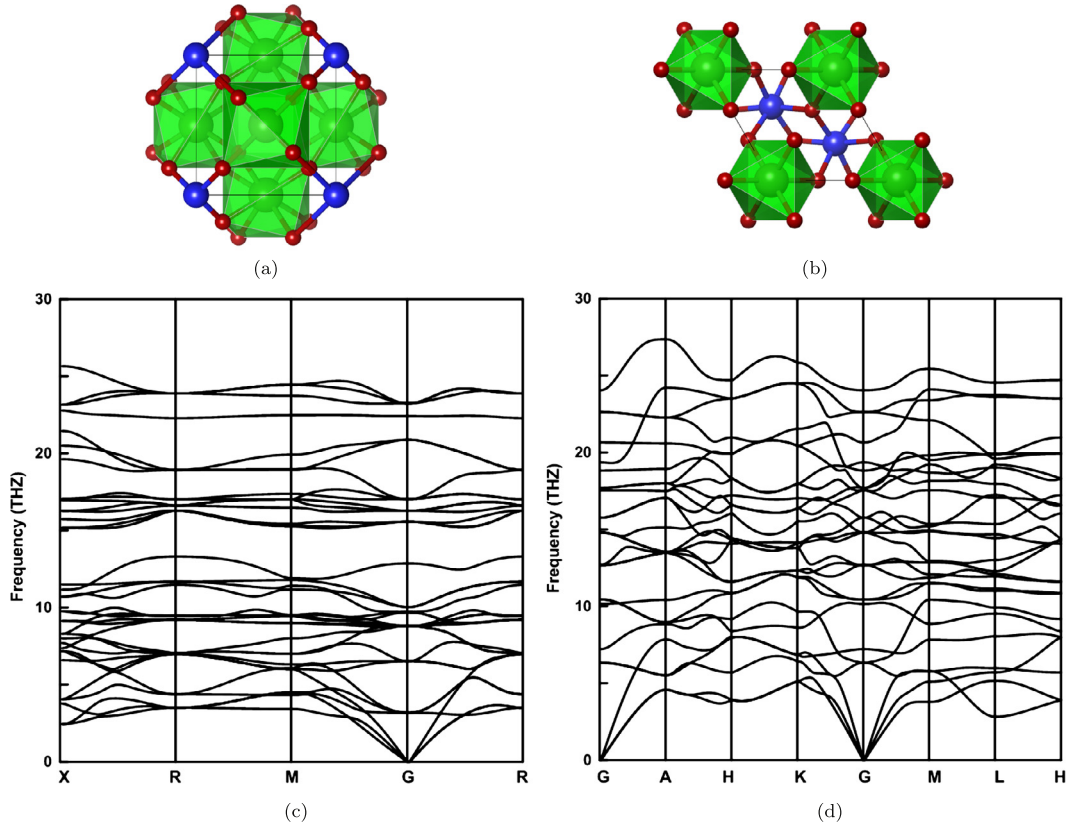
Fig. 2. (Color online.) Crystal structure of (a) $P\bar{4}3m$-Zr_3SiO_8, Zr is at $3c$ (0.5, 0, 0.5); Si at $1a$ (0, 0, 0); O1 at $4e$ (0.1924, 0.8076, 0.8075); O2 at $4e$ (0.3042, 0.6958, 0.3042) and (b) $P\bar{3}1m$-$ZrSi_2O_6$, Zr is at $1a$ (0, 0, 0); Si at $2d$ (0.3333, 0.6667, 0.5); O at $6k$ (0.3626, 0.3626, 0.2847) at ambient pressure. Phonon dispersion curves of (c) $P\bar{4}3m$-Zr_3SiO_8; and (d) $P\bar{3}1m$-$ZrSi_2O_6$ at ambient pressure. Green spheres (contained in the green polyhedra) show Zr atoms; blue spheres – Si; red spheres – O. Polyhedra show the coordination of Zr atoms (8-fold in Zr_3SiO_8, and 6-fold in $ZrSi_2O_6$).

Table 1
Crystallographic data and enthalpies of the formation of zirconium silicates.

Compound	Enthalpy of formation (eV/atom)	Space group	Lattice constants (Å)
$ZrSiO_4$	0	$I4_1/amd$	$a = 6.700$
			$c = 6.012$
			$a = 6.708$ [31]
			$c = 6.04$
Zr_3SiO_8	0.074	$P\bar{4}3m$	$a = 5.073$
$ZrSiO_4$	0.079	$I4_1/a$	$a = 4.777$
			$c = 10.596$
			$a = 4.786$ [32]
			$c = 10.659$
$ZrSi_2O_6$	0.147	$P\bar{3}1m$	$a = 4.689$
			$c = 4.584$

$$\max F_{ED} = \frac{1}{2}\varepsilon_0 k E_{BI}^2 = 8.1882 \text{ J/cm}^3 \times k(E_g/E_{gc})^{2\alpha}, \quad (1)$$

The compositional dependence of the electric energy density of the crystal structures highlighted by USPEX is shown in Fig. 4. The tetragonal ZrO_2 ($P4_2/nmc$) has the highest energy density (406.3 J/cm^3) among a number of crystalline forms of ZrO_2. The tetragonal SiO_2 ($I4_1/amd$), which was reported before [3], has the highest energy density (163.7 J/cm^3) among SiO_2 polymorphs. It is noteworthy that the ZrO_2–SiO_2 compound with the highest energy density (128.55 J/cm^3) is $ZrSiO_4$ ($I4_1/a$); this is due to its much higher permittivity (15.70) and reasonably large band gap (4.0 eV). Thus, as it emerges from our theoretical calculation, $I4_1/a$-$ZrSiO_4$ is a good candidate for Zr-based dielectrics for electronic applications, e.g. in CMOS devices.

Average static dielectric constant κ, band gap E_g, intrinsic breakdown field E_{BI} and energy density F_{ED} of $I4_1/amd$-$ZrSiO_4$,

$I4_1/a$-$ZrSiO_4$, $P\bar{4}3m$-Zr_3SiO_8 and $P\bar{3}1m$-$ZrSi_2O_6$ are presented in Table 2. In the framework of DFT–GGA calculation, $P\bar{4}3m$-Zr_3SiO_8 has the highest average static dielectric constant (20.70). The difference in the static dielectric constant between HfO_2–SiO_2 (11–21) [9] and ZrO_2–SiO_2 (12–20) is minor, while the bandgap of HfO_2–SiO_2 (4.4–5.4 eV) [9] is higher than ZrO_2–SiO_2 (3.5–4.5 eV). Therefore, HfO_2–SiO_2 (130–236 J/cm^3) [9] compounds have a higher energy density fitness than ZrO_2–SiO_2 (77–129 J/cm^3) on the whole.

Colorless zircon is a popular substitute for diamond, because of its high refractive index, which can be expressed by the following equations:

$$R = n + in(im), \quad (2)$$

$$n = \sqrt{\frac{\sqrt{\varepsilon_1^2 + \varepsilon_2^2} + \varepsilon_1}{2}}, \quad (3)$$

$$n(im) = \sqrt{\frac{\sqrt{\varepsilon_1^2 + \varepsilon_2^2} - \varepsilon_1}{2}}, \quad (4)$$

where R represents the complex refractive index with the real part n and imaginary parts $n(im)$. ε_1 and ε_2 are, respectively, the real part and the imaginary part of the dielectric function. In our work, we are mostly concerned with the real part of the refractive index and ignore its imaginary part because the imaginary part k is almost zero in the visible-light frequency range (1.66 eV–3.27 eV). Fig. 5 shows the frequency dependence of the refractive indices of $I4_1/amd$-$ZrSiO_4$, $I4_1/a$-$ZrSiO_4$, $P\bar{4}3m$-Zr_3SiO_8 and $P\bar{3}1m$-$ZrSi_2O_6$ in the visible-light frequency range. The result indicates that
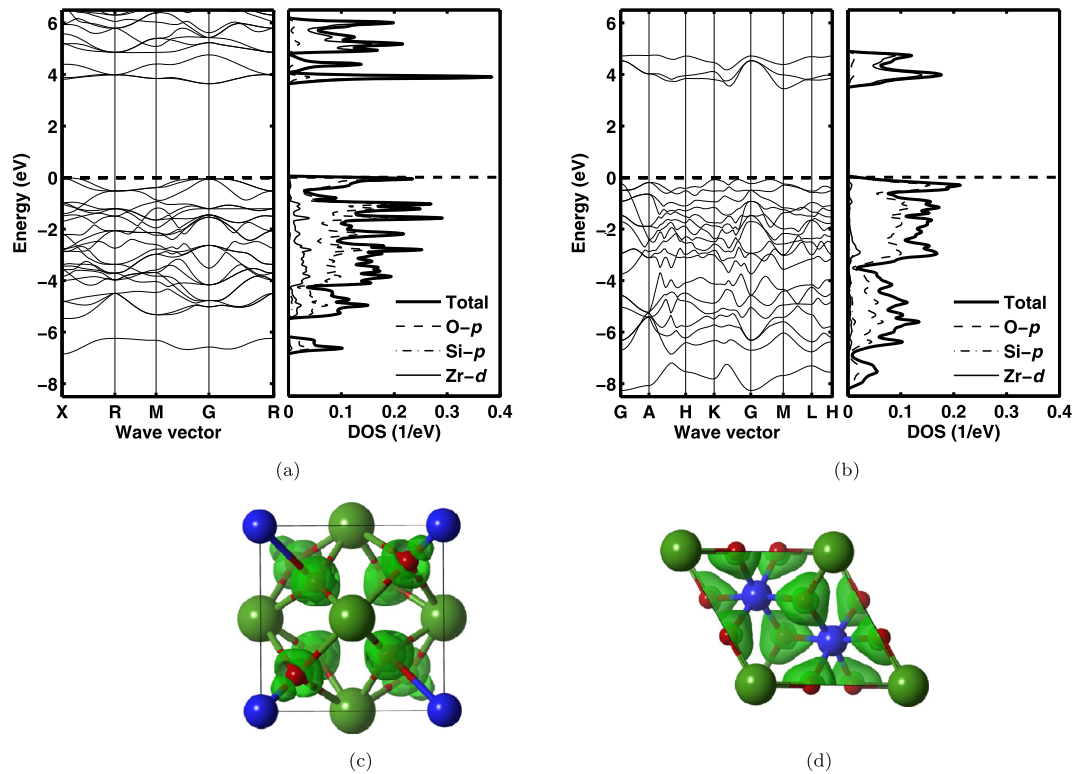
Fig. 3. (Color online.) Band structure and partial densities of states for (a) Zr_3SiO_8 and (b) $ZrSi_2O_6$. The Fermi energy is set to zero. (c) ELF isosurface of Zr_3SiO_8 for ELF = 0.815; (d) ELF isosurface of $ZrSi_2O_6$ for ELF = 0.756. Green spheres show Zr atoms; blue spheres – Si; red spheres – O.

Table 2
Electronic and static dielectric tensors, average static dielectric constant κ, band gap E_g, intrinsic breakdown field E_{BI} and energy density F_{ED} of the ZrO_2–SiO_2 polymorphs.

Compound space group	Dielectric tensor (components: 11 22 33)		κ	E_g (eV)	E_{BI} (V/nm)	F_{ED} (J/cm^3)
	ε^0	ε^∞				
$ZrSiO_4$ $I4_1/amd$	[12.61 12.50 12.72]	[4.31 4.47 4.21]	12.61 13 [8]	4.43 4.45 [33] 6.50 [12]	1.51	125.84
Zr_3SiO_8 $P\bar{4}3m$	[20.71 20.74 20.66]	[5.19 5.19 5.19]	20.70	3.65	1.03	97.99
$ZrSiO_4$ $I4_1/a$	[16.55 16.54 14.01]	[4.67 4.67 4.63]	15.70	4.00 4.02 [32]	1.36	128.55
$ZrSi_2O_6$ $P\bar{3}1m$	[19.62 19.78 21.42]	[4.16 4.16 4.51]	20.27	3.52	0.92	77.06

$P\bar{4}3m$-Zr_3SiO_8 has the highest refractive index (2.34–2.54) compared with the other three structures. Zr_3SiO_8 can be written as $(ZrO_2)_3$–(SiO_2), so it is a high concentration of ZrO_2 ($n = 2.13$–2.20 [30]) that makes Zr_3SiO_8 have such a high refractive index. If Zr_3SiO_8 can be synthesized, it can exhibit both a strong luster (due to high refractive index) and strong color effects (due to large dispersion of light).

4. Conclusions

In summary, we have performed searches for stable phases and for materials with maximum electric energy density fitness in the ZrO_2–SiO_2 system at ambient pressure using variable-composition evolutionary algorithm. In addition to the well-known compounds, $I4_1/amd$-$ZrSiO_4$ and $I4_1/a$-$ZrSiO_4$, we also found two other stoichiometric compounds, $P\bar{4}3m$-Zr_3SiO_8 and $P\bar{3}1m$-$ZrSi_2O_6$. All of these phases have a significantly ionic bonding character and are insulators. $P\bar{4}3m$-Zr_3SiO_8 and $P\bar{3}1m$-$ZrSi_2O_6$ have the higher dielectric constants among Zr-based materials. If we simultaneously optimize the delectric constant, bandgap and breakdown field, $I4_1/a$-$ZrSiO_4$ and $I4_1/amd$-$ZrSiO_4$ are both excellent energy stor-
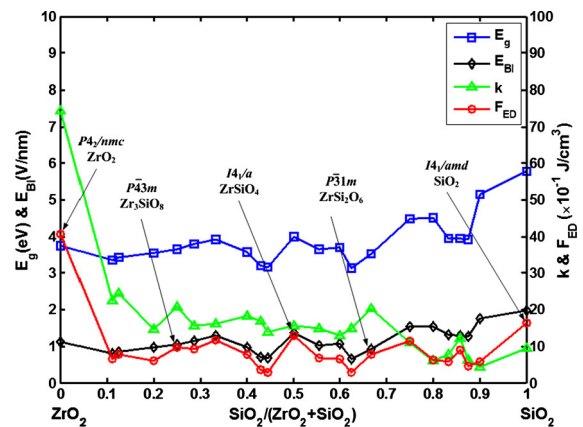

Fig. 4. DFT band gap (E_g), breakdown field (E_{BI}), dielectric permittivity (κ), and energy density fitness (F_{ED}) for representative ZrO_2–SiO_2 compounds.

age materials for electronic applications. $P\bar{4}3m$-Zr_3SiO_8 can be an interesting optical material or a gemstone due to its high refractive index ($\sim$2.4) and dispersion of light.
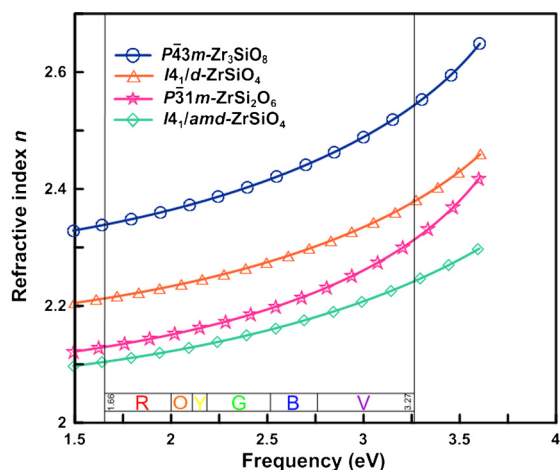
Fig. 5. Refractive index as a function of frequency of the investigated crystal structures of ZrO_2–SiO_2 polymorphs.

Acknowledgements

References

[1] X.D. Xiang, X. Sun, G. Briceno, Y. Lou, K.-A. Wang, H. Chang, W.G. Wallace-Freedman, S.-W. Chen, P.G. Schultz, A combinatorial approach to materials discovery, Science 268 (5218) (1995) 1738–1740.

[2] M.L. Green, I. Takeuchi, J.R. Hattrick-Simpers, Applications of high throughput (combinatorial) methodologies to electronic, magnetic, optical, and energy-related materials, J. Appl. Phys. 113 (2013) 231101.

[3] A. Jain, S.P. Ong, G. Hautier, W. Chen, W.D. Richards, S. Dacek, S. Cholia, D. Gunter, D. Skinner, G. Ceder, K.A. Persson, The materials project: a materials genome approach to accelerating materials innovation, Appl. Phys. Lett. Mater. 1 (1) (2013) 011002.

[4] G. Orange, G. Fantozzi, F. Cambier, C. Leblud, M. Anseau, A. Leriche, High temperature mechanical properties of reaction-sintered mullite/zirconia and mullite/alumina/zirconia composites, J. Mater. Sci. 20 (7) (1985) 2533–2540.

[5] J.F. Shackelford, W. Alexander, CRC Materials Science and Engineering Handbook, CRC Press, 2010.

[6] D.C. Cranmer, Fiber coating and characterization, Am. Ceram. Soc. Bull. 68 (2) (1989) 415–419.

[7] J. Feng, D. Chen, W. Ni, S. Yang, Z. Hu, Study of Ir absorption properties of fumed silica–opacifier composites, J. Non-Cryst. Solids 356 (9) (2010) 480–483.

[8] J. Choi, Y. Mao, J. Chang, Development of hafnium based high-k materials—a review, Mater. Sci. Eng. R 72 (6) (2011) 97–136.

[9] Q. Zeng, A.R. Oganov, A.O. Lyakhov, C. Xie, X. Zhang, J. Zhang, Q. Zhu, B. Wei, I. Grigorenko, L. Zhang, et al., Evolutionary search for new high-k dielectric materials: methodology and applications to hafnia-based oxides, Acta Crystallogr., Sect. C: Struct. Chem. 70 (2) (2014) 76–84.

[10] W.J. Qi, R. Nieh, E. Dharmarajan, B.H. Lee, Y. Jeon, L. Kang, K. Onishi, J.C. Lee, Ultrathin zirconium silicate film with good thermal stability for alternative gate dielectric application, Appl. Phys. Lett. 77 (11) (2000) 1704–1706.

[11] W.B. Blumenthal, The Chemical Behavior of Zirconium, van Nostrand, Princeton, NJ, 1958.

[12] J. Robertson, Band structures and band offsets of high k dielectrics on Si, Appl. Surf. Sci. 190 (1) (2002) 2–10.

[13] A.R. Oganov, Y. Ma, A.O. Lyakhov, M. Valle, C. Gatti, Evolutionary crystal structure prediction as a method for the discovery of minerals and materials, Rev. Mineral. Geochem. 71 (1) (2010) 271–298.

[14] A.R. Oganov, A.O. Lyakhov, M. Valle, How evolutionary crystal structure prediction works and why, Acc. Chem. Res. 44 (3) (2011) 227–237.

[15] A.R. Oganov, C.W. Glass, Crystal structure prediction using ab initio evolutionary techniques: principles and applications, J. Chem. Phys. 124 (24) (2006) 244704.

[16] A.O. Lyakhov, A.R. Oganov, H.T. Stokes, Q. Zhu, New developments in evolutionary structure prediction algorithm USPEX, Comput. Phys. Commun. 184 (4) (2013) 1172–1182.

[17] J.P. Perdew, K. Burke, M. Ernzerhof, Generalized gradient approximation made simple, Phys. Rev. Lett. 77 (18) (1996) 3865.

[18] G. Kresse, J. Furthmüller, Efficient iterative schemes for ab initio total-energy calculations using a plane-wave basis set, Phys. Rev. B 54 (16) (1996) 11169.

[19] P.E. Blöchl, Projector augmented-wave method, Phys. Rev. B 50 (24) (1994) 17953.

[20] H.J. Monkhorst, J.D. Pack, Special points for Brillouin-zone integrations, Phys. Rev. B 13 (12) (1976) 5188–5192.

[21] A. Togo, F. Oba, I. Tanaka, First-principles calculations of the ferroelastic transition between rutile-type and $CaCl_2$-type SiO_2 at high pressures, Phys. Rev. B 78 (13) (2008) 134106.

[22] R.F.W. Bader, Atoms in Molecules: A Quantum Theory, Oxford University Press, Oxford, 1990.

[23] G. Henkelman, A. Arnaldsson, H. Jónsson, A fast and robust algorithm for Bader decomposition of charge density, Comput. Mater. Sci. 36 (3) (2006) 354–360.

[24] A.R. Oganov, J. Chen, C. Gatti, Y. Ma, Y. Ma, C.W. Glass, Z. Liu, T. Yu, O.O. Kurakevych, V.L. Solozhenko, Ionic high-pressure form of elemental boron, Nature 457 (7231) (2009) 863–867.

[25] W. Zhang, A.R. Oganov, A.F. Goncharov, Q. Zhu, S.E. Boulfelfel, A.O. Lyakhov, E. Stavrou, M. Somayazulu, V.B. Prakapenka, Z. Konôpková, Unexpected stable stoichiometries of sodium chlorides, Science 342 (6165) (2013) 1502–1505.

[26] C.H. Hu, A.R. Oganov, Q. Zhu, G.-R. Qian, G. Frapper, A.O. Lyakhov, H.-Y. Zhou, Pressure-induced stabilization and insulator–superconductor transition of BH, Phys. Rev. Lett. 110 (16) (2013) 165504.

[27] C. Howard, R. Hill, B. Reichert, Structures of ZrO_2 polymorphs at room temperature by high-resolution neutron powder diffraction, Acta Crystallogr., Sect. B Struct. Sci. 44 (2) (1988) 116–120.

[28] T. Demuth, Y. Jeanvoine, J. Hafner, J. Angyan, Polymorphism in silica studied in the local density and generalized-gradient approximations, J. Phys. Condens. Matter 11 (19) (1999) 3833.

[29] A.D. Becke, K.E. Edgecombe, A simple measure of electron localization in atomic and molecular systems, J. Chem. Phys. 92 (1990) 5397.

[30] M. Jerman, Z. Qiao, D. Mergel, Refractive index of thin films of SiO_2, ZrO_2, and HfO_2 as a function of the films' mass density, Appl. Opt. 44 (15) (2005) 3006–3012.

[31] B.A. Kolesov, C.A. Geiger, T. Armbruster, The dynamic properties of zircon studied by single-crystal X-ray diffraction and Raman spectroscopy, Eur. J. Mineral. 13 (5) (2001) 939–948.

[32] M. Akhtar, S. Waseem, Computational study of scheelite ($ZrSiO_4$) by employing static simulation techniques, Solid State Sci. 5 (2003) 541–548.

[33] T.T. Jiang, Q.Q. Sun, Y. Li, J.J. Guo, P. Zhou, S.J. Ding, D.W. Zhang, Towards the accurate electronic structure descriptions of typical high-constant dielectrics, J. Phys. D, Appl. Phys. 44 (18) (2011) 185402.